World Academy of Science, Engineering and Technology
International Journal of Mechanical and Mechatronics Engineering
Vol:8, No:1, 2014

Phase-Averaged Analysis of Three-Dimensional Vorticity in the Wake of Two Yawed Side-By-Side Circular Cylinders

T. Zhou, S. F. Mohd. Razali, Y. Zhou, H. Wang, L. Cheng

***Abstract*—**Thewake flow behind two yawed side-by-sidecircular cylinders is investigated using athree-dimensional vorticity probe. Four yaw angles (α), namely, 0°, 15°, 30° and 45° and twocylinder spacing ratios T^* of 1.7 and 3.0 were tested. For T^* = 3.0, there exist two vortex streets and the cylinders behave as independent and isolated ones. The maximum contour value of the coherent streamwise vorticity $\widetilde{\omega}_x^*$ is only about 10% of that of the spanwise vorticity $\widetilde{\omega}_z^*$. With the increase of α, $\widetilde{\omega}_x^*$ increases whereas $\widetilde{\omega}_z^*$ decreases. At α = 45°, $\widetilde{\omega}_x^*$ is about 67% of $\widetilde{\omega}_z^*$.For T* = 1.7, only a single peak is detected in the energy spectrum. The spanwise vorticity contours have an organized pattern only at α = 0°. The maximum coherent vorticity contours of $\widetilde{\omega}_x^*$ and $\widetilde{\omega}_z^*$ for T^* = 1.7 are about 30% and 7% of those for T^* = 3.0.The independence principle (IP)in terms of Strouhal numbers is applicable in both wakes when α< 40°.

***Keywords*—**Circular cylinder wake, vorticity, vortex shedding.

I. Introduction

WHEN a fluid flows over a bluff body at a sufficiently high Reynolds number *Re* (≡ $U_\infty d/\nu$, where U_∞ is the free-stream velocity in the streamwise direction, d is the cylinder diameter and ν is the kinematic viscosity of the fluid), vortex shedding occurs, which results in time-dependent in-line and transverse forces. These forces will induce vibrations to the bluff body when the vortex shedding frequency is close to its natural frequency. This phenomenon is known as vortex-induced vibration (VIV). VIV is one of the most important aspects that should be avoided in engineering applications as it will contribute to the instability and fatigue damage to the structures. Thus, the studies in understanding the flow over bluff bodies are important in engineering applications, such as fluid flow across heat exchangers, air flow around high-rise buildings and yaw-cables of bridges. These studies would have benefits in understanding the vortex structures to minimize many problems associated with VIV and to improve the efficiency in maintaining the structures.

Whereas vortex shedding from a single cylinder is well documented both in air and in water flows, fluid flows over two identical cylinders is a far more complicated problem than that of the single cylinder. Over the past decades, many researchers have contributed to better understanding the flow around a pair of cylinders in a side-by-side arrangement [1]-[6]. There are many major parameters that may be responsible for vortex shedding from two cylinders arranged side-by-side with normal velocity incidence (i.e. the flow is perpendicular to the cylinders), such as initial condition, pressure distribution and Reynolds number [2],[3],[6]. Besides the parameters mentioned above, the vortex structures are also influenced by the centre-to-centre cylinder spacing ratio T^* (hereafter, a superscript asterisk denotes normalization by the diameter d and/or free-stream velocity U_∞). Various flow patterns and behaviors have been identified as the cylinder spacing ratio T^* is varied. For example, the variation of T^* from small to large could contribute to the formation of a single or multiple wakes. At large cylinder spacing ratio ($T^* \geq 2$), two coupled vortex streets have been observed with a definite phase relationship [7]. Based on [6], the two streets may occur in phase or in anti-phase. The two in-phase streets were anti-symmetrical about the flow centerline but symmetrical for the anti-phase case. The in-phase vortex streets eventually merged downstream to form a single street, whereas the anti-phase streets remained distinct farther downstream. He found that for $2 < T^* < 6$, the vortex shedding was predominant in anti-phase. At intermediate cylinder spacing $1.2 < T^* < 2.0$, the flow behind two cylinders produced two bi-stable wakes, one narrow and the other wide. The flow was flip-flopping and randomly changed from one side to the other because of the bi-stable deflected flow between the cylinders [4], [8], [9]. By using a phase-averaging method, Reference [3] found that the longitudinal and lateral spacing between vortices for T^* = 1.5 were larger than those for $T^* = \infty$ and 3.0. Large lateral spacing ratio implies a weak interaction between vortical motions that may account for the long lifespan and the stability of the vortex street. They proposed that for T^*= 1.5, the vortices developed from the shear layer instability in the wide wake leading to the early disappearance of the narrow wake. The dominant frequency in the narrow wake was about triple that in the wide wake [4], which was caused by the flip-flopped flow due to the

T. Zhou is with School of Civil and Resource Engineering, The University of Western Australia, 35 Stirling Highway, WA 6009, Australia (Phone: 61-8-64887094; fax: 61-8-64881018. e-mail: tongming.zhou@uwa.edu.au).

S. F. Mohd. Razaliis with Department of Civil and Structural Engineering, Faculty of Engineering and Built Environment, Universiti Kebangsaan Malaysia, 43600 UKM Bangi, Selangor, Malaysia (e-mail: fatin@eng.ukm.my)

Y. Zhou is with Institute for Turbulence-Noise-Vibration Interaction and Control, Shen Zhen Graduate School, Harbin Institute of Technology, P R China (e-mail: zhouyu@hitsz.edu.cn).

H. Wang is with School of Civil Engineering and Architecture, Central South University, Changsha, P. R. China (e-mail:wanghfme@gmail.com)

L. Cheng is with School of Civil and Resource Engineering, The University of Western Australia, 35 Stirling Highway, WA 6009, Australia (e-mail: liang.cheng@uwa.edu.au).

squeezing effect and amalgamation of the vortices generated behind the cylinders [7]. They suggested that the vortices in the narrow wake had a tendency to pair and absorb the vortex from the wide wake. Reference [10] showed that at $T^* < 1.2$, the wake of two side-by-side circular cylinders generateda single vortex street similar tosingle bluff body behavior. However, the peak frequency in the power spectrum of the former was lower than that of the latter.

Although many studies have been conducted in both large and intermediate cylinder spacing ratios, none of them measured the three vorticity components simultaneously. Furthermore, the previous studies focused only on the cross-flow case where the cylinder was perpendicular to the on-coming flow. In practical engineering applications, this is not always the case. More often, the cylinders are yawed to the on-coming flow. In the present study, the yaw angle is defined as the angle between the oncoming flow direction and the direction which is perpendicular to the cylinder axis so that $\alpha = 0°$ corresponds to the cross-flow case whereas $\alpha = 90°$ corresponds to the axial flow case (see Fig. 1 (a)). The flow structures and vortex shedding for a single yawed cylinder have been studied previously by a number of investigators [11]-[14]. It has been shown that the vortex shedding frequency of a yawed cylinder behaves in a similar way to normal-incidence case through the use of the component of the free-stream velocity normal to the cylinder axis. If the force coefficients and the Strouhal number are normalized by the velocity component normal to the cylinder axis ($St_N \equiv f_0 d/U_N$, where f_0 is the vortex shedding frequency and $U_N \equiv U_\infty \cos\alpha$), the values are approximately independent of α. This is often known in the literature as the independence principle (IP) or the Cosine Law. For a single cylinder wake, several theoretical and experimental studies have verified the IP [15], [16]. However, many studies showed deviations from the IP [12], [14], [17]-[23], especially at large yaw angles. It has been suggested that the IP was valid for $\alpha \leq 35°–40°$ [13], [18], [23], [24] whereas for larger α, the IP was not valid because the shedding frequency was smaller than that predicted by the IP and the vortex slant angle was less than the cylinder yaw angle [22].

In this paper, the flow structures in the wake of two yawed cylinders with cylinder spacing ratios $T^* = 3.0$ and 1.7 are investigated, which represent the large ($T^* \geq 2$) and intermediate ($1.2 < T^* < 2$) cylinder spacing, respectively. In the experiments, the three vorticity components in the wake were measured simultaneously using a three-dimensional multi-hotwire vorticity probe at a free-stream velocity (U_∞) of 8.5 m/s, corresponding to a Reynolds number $Re = 7200$, at which the flow can be classified as in the turbulent regime. Therefore, it is important to measure all three vorticity components simultaneously to provide more completed data for studying turbulence characteristics than using simpler probe geometries. Although there are some published experimental data on turbulence characteristics in the wake behind a pair of circular cylinders arranged side-by-side in a cross-flow, there is no study on the three-dimensional vorticity characteristics in the wake behind yawed cylinders arranged side-by-side. Therefore, to gain some more fundamental understanding of the flow structures in the intermediate wake region, all three velocity and vorticity components in the wake of two yawed cylinders arranged side-by-side for cylinder spacing ratios $T^* = 3.0$ and 1.7 were measured simultaneously using a multiple hotwire vorticity probe. Based on the data, the effects of the yaw angle α and the cylinder spacing ratio T^* on turbulence characteristics and vortical structures can be examined in detail.

II. Experimental Details

A. Experimental Arrangement

The measurements were conducted in a closed loop wind tunnel with a test section of 1.2m (width) × 0.8m (height) and 2m in length. The free-stream velocity in the test section was uniform to within 0.5% and the free-stream turbulence intensity was less than 0.5%. Two identical circular cylinders arranged side-by-side with a diameter $d = 12.7$mm were used to generate the wake flow. The cylinders were installed horizontally at the centre of the test section and supported rigidly at both ends by two aluminum end plates to minimize the side effects to the wake flow. Two cylinder spacing ratios $T^* = 3.0$ and 1.7, were tested. For each case, four yaw angles, namely $\alpha = 0°$, 15°, 30° and 45°, were tested at downstream locations $x^* = 10$, 20 and 40. However, in this paper, only results at $x^* = 10$ are shown and discussed. The arrangement of the cylinder and the definition of the coordinate system are shown in Fig. 1 (a). As shown in the figure, the coordinate system is defined as the x-axis is in the same direction as the incoming flow located at the centre of the transverse spacing of both cylinders. The y-axis is perpendicular to the x-axis in the vertical plane coming through the cylinders (another cylinder cannot be seen in the plan view) and out of the paper whereas the z-axis is normal to both x- and y- axes.

The vorticity probe was moved along the y-direction to measure simultaneously the three-dimensional velocity components. AnX-probe was fixed at $y = 4d$ to provide a phase reference for the measured signals by the moveable vorticity probe. The vorticity probe consisted of 4 X-probes (X-probes A, B, C and D) as shown in Figs. 1 (c), (d). Both X-probes A (wires 1 and 2) and C (wires 5 and 6) which aligned in the x-z plane and separated in the y-axis (Δy) measure u and w velocity signals whereas X-probes B (wires 3 and 4) and D (wires 7 and 8) which aligned in the x-y plane and separated in the z-axis (Δz) measure u and v velocity signals. The separations between the centres of the two opposite X-probes (Δy and Δz) were about 2.7mm. The clearance between the two hotwires for each X-probe was about 0.7mm. The hotwires of the vorticity probe were etched from Wollaston (Pt-10% Rh) wires. The active length was etched to about $200d_w$, where the hotwire diameter d_w is about 2.5μm. The wires were operated on constant temperature circuits at an overheat ratio of 1.5. The angle calibration was carried out at ±20°. The included angle of each X-probe was about 110° and the effective angle of the inclined wires was about 35°. All output signals were low-pass filtered at a cut-off frequency $f_c = 5200$ Hz and sampled at a frequency $f_s = 10400$ Hz using a 16 bit A/D converter. The record duration

for each measurement point was about 20s.

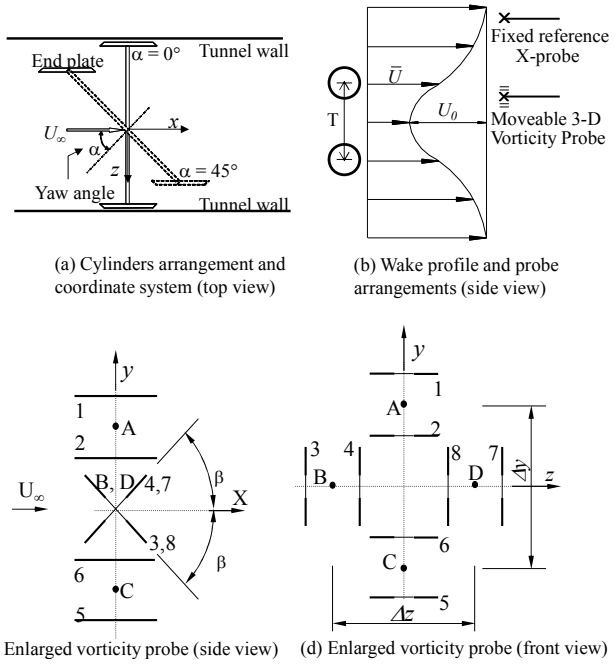

(a) Cylinders arrangement and coordinate system (top view)

(b) Wake profile and probe arrangements (side view)

(c) Enlarged vorticity probe (side view)

(d) Enlarged vorticity probe (front view)

Fig. 1 Two side-by-side cylinders with definitions of the coordinate system and the sketches of the vorticity probe.

From the velocity signals obtained through the experiments, the vorticity components can be calculated via,

$$\omega_x = \frac{\partial w}{\partial y} - \frac{\partial v}{\partial z} \approx \frac{\Delta w}{\Delta y} - \frac{\Delta v}{\Delta z}, \quad (1)$$

$$\omega_y = \frac{\partial u}{\partial z} - \frac{\partial w}{\partial x} \approx \frac{\Delta u}{\Delta z} - \frac{\Delta w}{\Delta x}, \quad (2)$$

$$\omega_z = \frac{\partial v}{\partial x} - \frac{\partial (\bar{U} + u)}{\partial y} \approx \frac{\Delta v}{\Delta x} - \frac{\Delta (\bar{U} + u)}{\Delta y}, \quad (3)$$

whereΔw and Δu in (1) and (3), respectively, are velocity differences measured by X-probes A and C; Δv and Δu in (1) and (2), respectively, are velocity differences measured by X-probes B and D. The velocity gradients $\Delta w/\Delta x$ and $\Delta v/\Delta x$ are obtained by using a central difference scheme to the time series of the measured velocity signals, e.g. $\Delta v/\Delta x \approx \Delta v/\Delta x \approx [v(i+1) - v(i-1)]/\Delta x$, where Δx is estimated based on Taylor's hypothesis given by $\Delta x = -U_c(2\Delta t)$. U_c is the vortex convection velocity and Δt ($\equiv 1/f_s$) is the time interval between two consecutive points in the time series of the velocity signals. A central difference scheme in estimating $\Delta w/\Delta x$ and $\Delta v/\Delta x$ is useful to avoid phase shifts between the velocity gradients involved in (2) and (3). The experimental uncertainty for $\bar{U}$ was about ±2%, whereas the uncertainties for u', v' and w' were about ±7%, ±8% and ±8%, respectively. Hereafter, a single over bar denotes conventional time-averaging and a superscript prime denotes root-mean-square values. More details of the vorticity probe were given in [13].

B. Phase-Averaging Method

The phase-averaging method is similar to that used by [3], [25], [26]. The v and v_r signals obtained from the moveable vorticity probe and the fixed reference probe, respectively, were band-pass filtered with the central frequency set at f_0 using a fourth-order Butterworth filter. The low-and high-pass frequencies were chosen to be the same value as f_0 so that the band-pass width of the filtered signal would be zero. More details about the phase-averaging method can be found in [3], [25] and [26].

III. Results And Discussion

A. Mean Streamwise and Spanwise Velocity Profiles

Fig.2 shows the time-averaged streamwise and spanwise velocity profiles, $\bar{U}^*$ and $\bar{W}^*$, of the wake at α = 0°, 15°, 30° and 45° for T^* = 3.0 and 1.7, respectively. The $\bar{U}^*$ profiles are generally symmetric about the wakecenterliney^* = 0. The trend of the $\bar{U}^*$ profile at α= 0° (Figs.2 (a), (b) are comparable with that reported by [5]. The variation in the magnitude of $\bar{U}^*$ between both studies may be because of the difference in Reynolds numbers which was about 5800 for the former study. The $\bar{U}^*$ profile displays a single peak around y^* = 0 for T^* = 1.7, which suggests the occurrence of a single vortex street at this separation, similar to that for $T^* = \infty$. The $\bar{U}^*$ profile for T^*= 3.0 displays a peak around y^* = 1.5 (the other peak is expected to be around $y^* = -1.5$) representing two vortex streets for T^* = 3.0. It is apparent that for T^* = 3.0 and at $y^* > 0$, $\bar{U}^*$ reveals a quite similar trend to that for $T^* = \infty$ at $y^* > -1.5$. This suggests that each vortex street of the former wake is similar to the single vortex street of the latter wake and the lateral distance between both vortices for the former wake is about 3d. For all spacing ratios, the magnitude of $\bar{U}^*$ at α = 0° is the smallest. With the increase of α, the magnitude of $\bar{U}^*$ increases gradually.

The maximum velocity deficit U_0^* and the wake half-width L^* for various yaw angles and cylinder spacing ratios are summarized in Table I. The wake half-width L is defined as the lateral distance from the wake centerline to the location where the velocity deficit equals to $\bar{U}^*$ /2. There is a significant reduction in U_0^* with the increase of α, regardless of the cylinder spacing. It can be seen that there is not much difference in the wake half-width L^* when α varies from 0° to 45° for both T^* = 3.0 and 1.7. The maximum difference is only about 5% which may be subject to the uncertainty in the experiments. This result is in contrast with that for $T^* = \infty$, where there is 15% decrease in L^* for $T^* = \infty$ when α changes from 0° to 45°, which cannot be attributed to the experimental uncertainty. It may imply that the L^*values for T^* = 3.0 and 1.7 are almost constant between various yaw angles.

The time-averaged spanwise velocity component $\bar{W}^*$ is one of the parameters used to assess the three-dimensionality of the

wake [27]. A larger value of $\overline{W}^*$ corresponds to the higher degree of three-dimensionality. The spanwise velocity acts to impair the two-dimensionality of the wake and hence vorticity strength [11],[14]. The values of $\overline{W}^*$ at various α for T^* = 3.0 and 1.7 are shown in Figs. 2 (c), (d). The profiles of $\overline{W}^*$ are generally symmetric about y^* = 0 for T^* = 3.0 (Fig. 2 (c)). It is shown that, at α = 0° and T^* = 3.0, $\overline{W}^*$ is almost zero across the wake. The trend is similar to that for single cylinder wake observed by [13]. This result is reasonable as for flow in normal direction to the cylinders, the flow is expected to have two-dimensional plane wake characteristics. With the increase of α, the magnitude of $\overline{W}^*$ (Figs. 2 (c), (d)) increases monotonously for y^*<2.8 and decreasing in the outer wake region, suggesting a stronger three-dimensionality with the increase of α. The maximum magnitude of $\overline{W}^*$ occurs at y^* = 1.5 for T^* = 3.0.

At T^* = 1.7, the $\overline{W}^*$ profiles (Fig.2 (d)) lack symmetry about y^* = 0, especially at α= 0°. In contrast to T^*= 3.0 and ∞, the value of $\overline{W}^*$ is not equal to zero even at α= 0°. This may be related with the gap flow between the cylinders. The numerical study by [7] suggested that the wake transition to turbulence in separating shear layer occurred at x^* = 1.5. Over the downstream wake location x^* = 10, due to the shear layer instability, the vortices are formed in the wide wake. The vortices in the narrow wake, caused by the wake deflection, have probably disappeared before x^* = 10 [3]. They suggested that the vortex evolution or regeneration was not completed yet at this streamwise region. With the increase of α to 15° (Fig.2 (d)), the symmetry about y^* = 0 is enhanced. When α further increases to 30° and 45° the symmetry is apparent at about y^* = -0.2 and -0.3, respectively. Also, with the increase of α, the magnitudes of $\overline{W}^*$ in the central region increases significantly, suggesting enhanced three-dimensionality of the wake.

As a larger $\overline{W}^*$ magnitude implies a higher degree of three-dimensionality, hence a stronger instability of the vortex filament [26], the variation of the normalized velocity gradient $\partial\overline{W}^*/\partial y^*$ implies the magnitude of the mean streamwise vorticity $\overline{\omega}_x(\equiv \partial\overline{W}/\partial y - \partial\overline{V}/\partial z)$. The distributions of $\partial\overline{W}^*/\partial y^*$ for T^* = 3.0 and 1.7 at different α are shown in Fig.3. At α = 0°, the distributions of $\partial\overline{W}^*/\partial y^*$ both for T^*=3.0 and 1.7 are close to zero. The absolute magnitudes of $\partial\overline{W}^*/\partial y^*$ for both T^*values increase with the increase of α. This result suggests a larger $\overline{\omega}_x$ with the increase ofα. The maximum magnitudes of $\partial\overline{W}^*/\partial y^*$ occur at around y^* = 2.0-2.2 and 1.2-1.4 for T^* = 3.0 and 1.7, respectively. Whereas the distributions of $\partial\overline{W}^*/\partial y^*$ provide a measure to the mean streamwise vorticity $\overline{\omega}_x$, the values of $\partial\overline{U}^*/\partial y^*$ provides a measure to the mean spanwise vorticity $\overline{\omega}_z$ $(\equiv \partial\overline{V}/\partial x - \partial\overline{U}/\partial y)$. The distributions of $\partial\overline{U}^*/\partial y^*$ at different α for both T^*values are also shown in Fig. 3. With increasing α, the magnitudes of $\partial\overline{U}^*/\partial y^*$ decrease gradually. This result indicates smaller values of $\overline{\omega}_z$ at larger α. In comparison amongT^* = ∞, 3.0 and 1.7, it can be seen that the magnitudes of $\partial\overline{W}^*/\partial y^*$ and $\partial\overline{U}^*/\partial y^*$ at T^* = 1.7 are the largest for all yaw angles whereas those for T^* = ∞ and 3.0 are comparable except those for T^* = 3.0 which are almost zero at around $y^* \approx 1.3$ instead at the wake centreline.

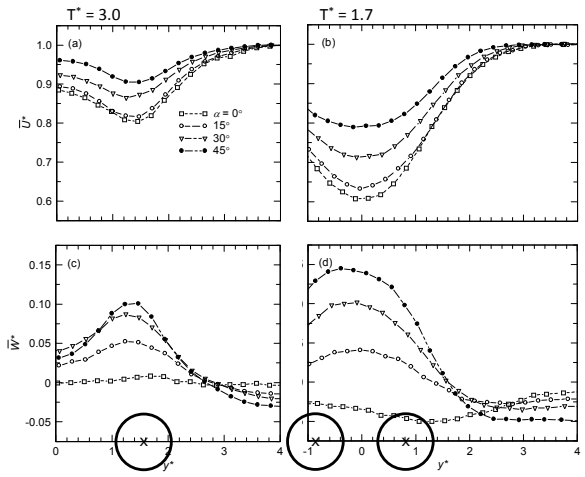

Fig. 2 Comparisons of time-averaged velocities at different yaw angles for T^* = 3.0 and 1.7. (a), (b) $\overline{U}^*$; (c), (d) $\overline{W}^*$. The open circles with a cross at the centre represent the locations of the cylinders.

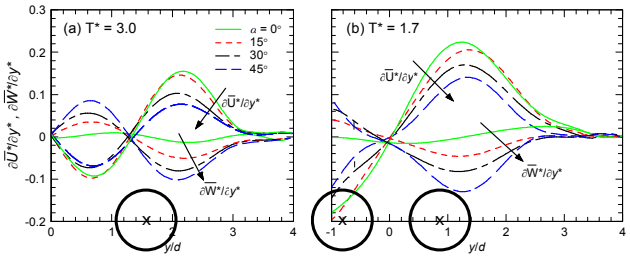

Fig. 3 Normalized velocity gradients at different yaw angles for (a) T^* = 3.0; (b) 1.7. The arrows indicate the direction of increasing yaw angles. The open circles with a cross at the centre represent the locations of the cylinders.

The shedding angle θ proposed by [28] can be used to evaluate if vortex shedding is oblique or not. They suggested that for oblique shedding, $\theta$was related to $\overline{\omega}_x$ and $\overline{\omega}_z$, whereθ=$\tan^{-1}(\overline{\omega}_x/\overline{\omega}_z)$ could be simplified further as θ= $\tan^{-1}(S_W/S_U)$ with S_W and S_U being the maximum velocity gradients of $\partial\overline{W}^*/\partial y^*$ and $\partial\overline{U}^*/\partial y^*$, respectively. Thus, the shedding angle θcan be calculated from the values of S_W and S_U inFig.3. The values ofθat different yaw angles for T^* = 3.0 and 1.7 are given in Table I. It is shown that for T^* = 3.0, θ is

slightly larger than the cylinder yaw angle α, indicating that the vortex is not exactly parallel to the cylinder. Whereas for $T^* = 1.7$, the values of $\theta$are quite close to α, suggesting that the vortices are almost parallel to the cylinder axis.

B. Power Spectra of Velocity and Vorticity Signals

The power spectra of the velocity and vorticity signals at $\alpha = 0°$ and 45° measured around $y^* = 1.5$ are shown in Figs.4 and 5, respectively. The results at $\alpha = 15°$ and 30° are not shown here as the spectra at these angles follow the trend when α varies from 0° to 45°. All power spectra are normalized to decibel scale by using the maximum values of ϕ_v or ϕ_{ω_z} at $\alpha = 0°$ and 45°, respectively. The *x*-axis in the figures is normalized to f_N ($\equiv fd/U_N$). This normalization allows the peak frequency $f_0$of the energy spectrum to correspond to the Strouhal number St_N ($\equiv f_0 d/U_N$). The values of St_N at different yaw angles for various cylinder spacing ratios are listed in Table I.For $T^* = 3.0$ at $\alpha = 0°$ (Fig. 4 (a)), each power spectrum of all velocity components *u*, *v* and *w*shows a discernible peak which corresponds to $St_N = 0.2$. The peak energy of ϕ_v is the highest, followed by ϕ_u and ϕ_w. The St_N for $T^* = 3.0$ is comparable to that for a single cylinder at all yaw angles (see Table I for comparison). As an example, at $\alpha = 0°$, $St_N = 0.2$ for $T^* = 3.0$ whereasit is 0.195 for $T^* = \infty$. The differences of St_N for both $T^* = 3.0$ and ∞ are around 5-11% for $\alpha < 40°$. In wakes of both $T^* = \infty$ and 3.0, the second harmonic of vortex shedding is pronounced in ϕ_u and ϕ_v. The minor peak is because of the occurrence of the second harmonic of vortex shedding [26]. With the increase of α to 45° (Fig. 4 (b)), the peak region is broadening over the frequency axis. The second harmonic peak also vanishes at this yaw angle. Reference [13] has shown that for a single cylinder wake, when α is smaller than 40°, the values of St_N keep approximately constant within the experimental uncertainty. For $T^* = 3.0$, the peak of $\phi_v$at $\alpha = 15°$, 30° and 45° is evident, which corresponds to $St_N = 0.212$, 0.220 and 0.246, respectively. The comparison of St_N between various yaw angles for $T^* = 3.0$ and 1.7 are shown in Fig.6. The ratio St_N/St_0 (St_0 represents the Strouhal number at $\alpha = 0°$) and the error bars are used in the figure to have a better visualization on the ratio $St_N/St_0$and the range of experimental uncertainty. The experimental uncertainty of St_N in the present study is estimated to be around ±8.5%. The results show that if a tolerance of ±8.5% is applied, the data support the IP for $\alpha < 40°$. Whereas for larger α, the deviation of St_N/St_0 from 1 is large and cannot be attributed to the experimental uncertainty. The above results indicate that the independence principle is applicable to side-by-side cylinder wake with $T^* = 3.0$ if$\alpha$is smaller than 40°.

For $T^* = 1.7$, the velocity spectrum at $\alpha = 0°$ (Fig.4 (c)) shows a dominant peak occurring at a frequency f_0 which corresponds to $St_N = 0.118$.Reference [7] detected two peaks in the energy spectra near $f_N = 0.16$ and 0.24 in their study of two side-by-side cylinder wakes with$T^* = 1.7$. The two peaks represent the Strouhal numbers for the wide and narrow wakes. The wide wake has a lowerStrouhal number whereas the narrow wake has a higherStrouhal number. The single peak observation may be because, at the downstream location $x^* = 10$, the vortex regeneration or evolution may not be completed yet. The other peak cannot be detected in the present study as the vortex in the narrow wake is probably diminished before this downstream location [3]. A similar observation has been made by [3], who reported a single dominant frequency across the wake, which corresponded to $St_N = 0.11$. A possible transition from the wide and narrow wake regimes to a single vortex street may finish at the present downstream location [3]. With the increase of α from 0° to 15°, 30° and 45°, the spectra exhibit a peak at a frequency which corresponds to $St_N = 0.122$, 0.119 and 0.133, respectively. The comparison of the St_N for $T^* = 1.7$ at $\alpha = 15°$, 30° and 45° with that at $\alpha = 0°$ is also given in Fig.6. It is shown that the values ofSt_N at $\alpha = 15°$ and 30° are within the experimental uncertainty. Therefore, the St_N can be considered as a constant. The difference (12.7%) of St_Nat $\alpha = 45°$ from that at $\alpha = 0°$ may not be ascribed to the experimental uncertainty. It may reflect a genuine departure in the IP when α is large. This observation is similar to that for the single cylinder results which may be because of the occurrence of the vortex evolutions from the wide and narrow regimes to a single vortex street. Therefore, the present study suggests that IP is applicable for $T^* = 1.7$ when $\alpha < 40°$.

The spanwise vorticity spectrum for $T^* = 3.0$ at $\alpha = 0°$ (Fig. 5 (a)) shows a significant peak at the vortex shedding frequency, implying large spanwise vortices in the wake. Similar to the single cylinder result, the transverse vorticity spectrum ϕ_{ω_y} does not show any peak whereas the streamwise vorticity spectrum ϕ_{ω_x} shows a very minor peak at f_0. The peak heights relative to the heights of the plateaux of ϕ_{ω_x} and ϕ_{ω_z} over the range of $f_N = 0.004$–0.1 are 3 dB and 16 dB, respectively. With the increase of α to 45° (Fig. 5 (b)), the peak of ϕ_{ω_z} is changed from sharp to broad. At this yaw angle, the peak height relative to the height of the plateaux of ϕ_{ω_x} and ϕ_{ω_z} over the range of f_N = 0.004–0.1 are 5 dB and 11 dB, respectively, suggesting a decrease in the spanwise vortex shedding intensity and an enhanced streamwise vortex shedding intensity. This result has the same trend as that for $T^* = \infty$ by [13], which can be related to the study by [29],who found that the increase of the streamwise vortices was at the expense of the primary spanwise vortices.

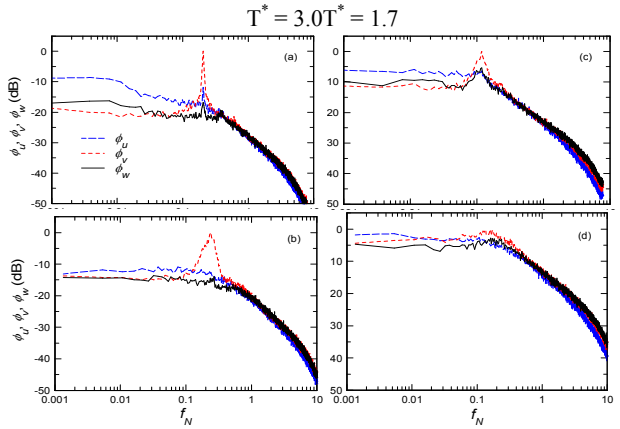

Fig. 4 Power spectra of *u*, *v* and *w*for different cylinder spacing ratios (a), (c): $\alpha = 0°$; (b), (d): 45°

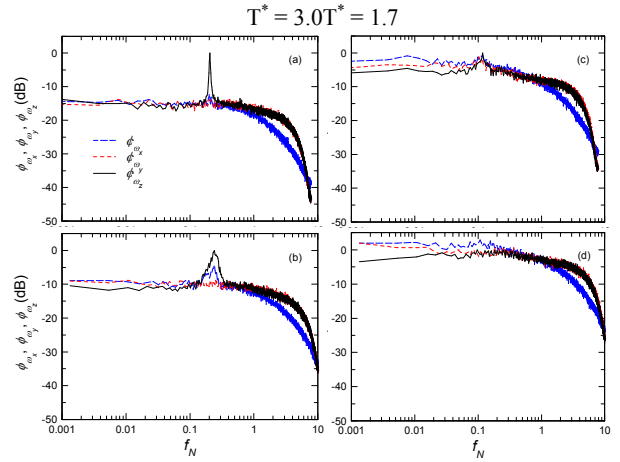

Fig. 5 Power spectra of ω_x, ω_y and$\omega_z$for different cylinder spacing ratios (a), (c): $\alpha = 0°$; (b), (d): 45°

The vorticity spectra ϕ_{ω_x} and ϕ_{ω_z} for $T^* = 1.7$ at $\alpha = 0°$ (Fig. 5 (c)) show minor peaks at the same f_0 as that of the velocity spectra (Fig. 4 (c)). However, compared with the peaks in Fig. 5 (a), the peaks in Fig. 5 (c) are much smaller. The peak heights relative to the plateaux of ϕ_{ω_x} and ϕ_{ω_z} are 2 dB and 5 dB, respectively.This result indicates that at $T^* = 1.7$, the vortex shed from the two cylinders is not as strong as that from both an isolated cylinder and two cylinders of a large spacing ratio (e.g. $T^* = 3.0$). The lack of an apparent sharp peak in Fig. 5 (c) is consistent with the trend of coherent vorticity contours (as shown in Fig. 8 later). The peak magnitudes of ϕ_{ω_x} and ϕ_{ω_z} are getting closer with increasing α, and at $\alpha = 45°$, no peaks can be identified on ϕ_{ω_x} and ϕ_{ω_z}. This result indicates that the three vorticity components are likely to have similar magnitudes and strength when α is increased, which will be confirmed later.

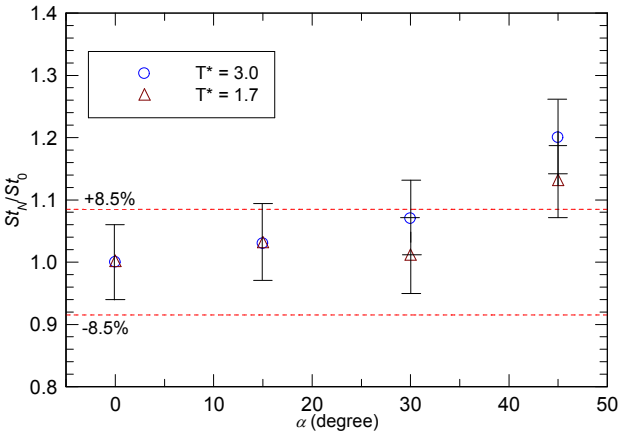

Fig. 6 Ratio of Strouhal number $St_N$to that at $\alpha = 0°$ for different cylinder spacing ratios. The horizontal dashed lines represent the range of experimental uncertainty

C. Phase-averaged Vorticity Fields

Figs. 7 and 8 present the contours of the phase-averaged vorticity components $\tilde{\omega}_x^*$, $\tilde{\omega}_y^*$ and $\tilde{\omega}_z^*$ for $T^* = 3.0$ and 1.7 at four yaw angles $\alpha = 0°$, 15°, 30° and 45°. The contours for $T^* = \infty$ were shown in [26] and will not be repeated here. The contours are in the (ϕ, y^*) plane, where the phase ϕ (from -2π to 2π) can be interpreted in terms of a streamwise distance and y^* (from 0 to 4.8 for $T^* = 3.0$ and from –1 to 4.8 for $T^* = 1.7$) is the transverse distance which is normalized by diameter. The flow direction is from left to right on the phase-averaged contours. The phase $\phi = 2\pi$ corresponds to the Kármán wavelength λ ($\equiv U_c/f_0$) or $\lambda/2$ ($\equiv U_c/2f_0$) for $T^* = 3.0$ and 1.7 contours, respectively, where U_c is the vortex convention velocity. The values for U_c are estimated with the values of $\overline{U} + \tilde{u}$ at the vortex centers [30]. The U_c and λvalues for different yaw angles and cylinder spacing ratios are included in Table I. It is evident that the wavelength λ of the Kármán vortices for T^* = 1.7 at all yaw angles are about 50-77% greater than those for T^* = 3.0 and ∞.

TABLE I
THE VORTEX SHEDDING ANGLE, MAXIMUM VELOCITY DEFECT, CONVECTION VELOCITY, HALF-WIDTH, NORMALIZED STROUHAL NUMBER AND WAVELENGTH AT DIFFERENT YAW ANGLES FOR CYLINDER SPACING RATIOS $T^* = \infty$ [26], 3.0 AND 1.7

	T^*	α			
		0°	15°	30°	45°
θ(°)	∞	0.5	16.8	33.0	45.6
	3.0	4.6	19.4	37.8	52.2
	1.7	3.9	12.6	25.8	42.9
U_0^*	∞	0.17	0.14	0.10	0.07
	3.0	0.20	0.19	0.13	0.10
	1.7	0.39	0.37	0.29	0.20
U_c^*	∞	0.82	0.83	0.87	0.89
	3.0	0.91	0.88	0.90	0.95
	1.7	0.86	0.76	0.83	0.86
L^*	∞	0.80	0.82	0.80	0.68
	3.0	2.57	2.53	2.53	2.69
	1.7	1.38	1.43	1.39	1.39
St_N	∞	0.195	0.202	0.206	0.224
	3.0	0.205	0.212	0.220	0.246
	1.7	0.118	0.122	0.119	0.133
λ^*	∞	4.16	4.23	4.80	5.86
	3.0	4.45	4.30	4.54	5.44
	1.7	7.29	6.44	8.05	9.14
λ^* (cosα)	∞	4.16	4.09	4.16	4.14
	3.0	4.45	4.15	3.93	3.85
	1.7	7.29	6.22	6.97	6.46
$\lvert\widetilde{\omega}_x^*\rvert$	∞	0.15	0.15	0.25	0.25
	3.0	0.05	0.15	0.20	0.20
	1.7	0.12	0.06	0.12	0.06
$\lvert\widetilde{\omega}_y^*\rvert$	∞	0.12	0.10	0.10	0.08
	3.0	0.10	0.10	0.12	0.08
	1.7	0.08	0.04	0.08	0.06
$\lvert\widetilde{\omega}_z^*\rvert$	∞	0.8	0.8	0.6	0.4
	3.0	0.70	0.60	0.60	0.30
	1.7	0.14	0.08	0.08	0.06

The phase-averaged $\widetilde{\omega}_z^*$ contours for $T^* = 3.0$ (Figs. 7 (i)-(l)) display remarkable periodicity, resulting from the Kármán vortex street for all yaw angles. The contours are symmetric with respect to the centerline $y^* = 0$. At all yaw angles, the vorticity contours display two distinct vortex streets and the magnitudes of the contours are smaller than those for $T^* = \infty$ [26]. Here, only a single vortex street is shown as the wake is symmetric about $y^* = 0$. Another vortex street is located below the centerline. The vortex centers at $\alpha = 0°$ are around $y^* = 1.3$ and 1.9 for the positive and negative vortices respectively, whereas those for $T^* = \infty$ are around $y^* = -0.2$ and 0.4. From the figure, it seems that if the whole set of the phase-averaged $\widetilde{\omega}_z^*$ contours for $T^* = 3.0$ were shifted downward by about $y^* = 1.5$, the vortex contours are quite similar with those for $T^* = \infty$ (figure shown in [26]). The maximum contour values of thespanwise vortices at $\alpha = 0°$ is –0.7 (Fig. 7 (i)). Even though there is a small decrease in the maximum contour value of $\widetilde{\omega}_z^*$ when αvaries from 0° to 30°, the variation is not very apparent. When $\alpha$is further increased to 45°, the maximum value of $\widetilde{\omega}_z^*$ decreases by about 50%. This observation suggests that the effect of yaw angle on the coherent spanwise vortices is greater when α> 30°. This may be caused by the increase of the spanwise velocity $\overline{W}^*$ as α increases (Fig.2).

The $\widetilde{\omega}_x^*$ contours for $T^* = 3.0$ (Figs. 7 (a)-(d)) exhibit organized patterns at all yaw angles. However, their strength are much weaker compared to those of $\widetilde{\omega}_z^*$. At $\alpha = 0°$, the size of the longitudinal vortices is much smaller than that of the spanwise vortices. The maximum magnitude of $\widetilde{\omega}_x^*$ at this yaw angle is only about 7% of that of $\widetilde{\omega}_z^*$, which is in agreement with the two-dimensionality of the flow. With the increase of yaw angles, the $\widetilde{\omega}_x^*$ contours exhibit more apparently organized patterns and the maximum contour value increases monotonously. This is consistent with that shown in Figs. 5 (a), (b) in that the peak height of ϕ_{ω_x} increases with increasing α. At $\alpha = 45°$, the maximum contour value of $\widetilde{\omega}_x^*$ (Fig.7 (d)) is about 67% of that of $\widetilde{\omega}_z^*$ (Fig.7 (l)). This result indicates the existence of the secondary axial vortices or the occurrence of vortex dislocation with an enhanced three-dimensionality when α increases, consistent with the result for a single cylinder wake [26]. Reference [26] suggested that the increase of the streamwise vorticity was caused by the increase of the spanwise velocity w at large yaw angles. This is because the calculation of ω_x is related with the velocity component w where the increase of w contributes to the increase of $\widetilde{\omega}_x^*$. The maximum value of $\widetilde{\omega}_y^*$ at $\alpha = 0°$ is about 2 times that of $\widetilde{\omega}_x^*$, which is still much smaller than that of $\widetilde{\omega}_z^*$. In comparison between the contours of $\widetilde{\omega}_x^*$ and $\widetilde{\omega}_z^*$ for $T^* = 3.0$, it can be seen that with the increase of α, the strength of the former increases whereas it decreases in the latter. The behavior of the streamwise and spanwise vortices is consistent with the result of the single cylinder wake by [26]. This result seems to support [29], who stated that the increase of the streamwise vortices is at the expense of the spanwise vortices. There is no apparent trend to be associated with the $\widetilde{\omega}_y^*$ contours when α increases from 0° to 45°. At $\alpha = 45°$, the maximum contour value of $\widetilde{\omega}_y^*$ is about half of that of $\widetilde{\omega}_x^*$. Overall, with the increase of α, the magnitudes and the pattern of $\widetilde{\omega}_x^*$ and $\widetilde{\omega}_z^*$ contours tend to be comparable whereas those of $\widetilde{\omega}_y^*$ are nearly unchanged. The maximum contour values of the coherent vorticity at different yaw angles for $T^* = 3.0$ are summarized in Table I.

The coherent vorticity contours for $T^* = 1.7$ are shown in Fig.8. All vorticity contours for this spacing obviously have distinctly different vortex patterns from the aforementioned wakes for $T^* = \infty$ and 3.0. Evidently, the $T^* = 1.7$ wake regime has a larger vortex wavelength λ compared to that for $T^* = \infty$ and 3.0. It can be seen that a single vortex street was shed from the top cylinder in the range from $y^* \approx -1$ to 3. The vortex structures in the wake are deflected downward below the wake centerline creating a wide wake. The lower part of the wake regime $y^* < -1$ may not be very important as it is believed that the vortex structures shed from the bottom cylinder have already vanished before $x^* = 10$ [3],[7]. Reference [30] in their

study of three side-by-side cylinders ($x^* \leq 10$ and $T^* = 1.5$) observed a wide wake behind the central cylinder and two narrow wakes on each side of the wide wake. They found that at $x^* \approx 5$, the vortex structures in the narrow wake on each side of the wide wake vanished whereas the vortex structures in the wide wake started to roll up. The vortex structures in the wide wake were very weak initially but became stronger with the streamwise direction which can be related to the shear layer instability [3]. The formation of the vortex street in the wide wake at further downstream region is also illustrated and briefly discussed by [6] through their numerical simulations for $T^* = 1.7$ at a low Reynolds number ($Re = 750$). They proposed the mechanisms involved in the vortex evolution of the wide and narrow wakes across the downstream region. Initially, the flow was deflected upwards creating a narrow wake around the top cylinder. The vortices in the narrow wake tend to pair and absorb the vortex from the bottom cylinder. Due to strong interaction between both vortices, the vortex shed from the bottom cylinder collapsed, thus encouraging the growth of the vortex from the top cylinder. As the vortex from the narrow wake (top cylinder) tends to prevent the merging of the following vortex from the wide wake (bottom cylinder), another vortex was created behind the bottom cylinder (now called a narrow wake). However, the vortex also quickly collapsed. At the same time, the vortex from the top cylinder becomes stronger and the flow deflected toward the bottom cylinder, creating a wide wake. Finally, a single vortex street was formed in the wide wake at the downstream location $x^* = 10$. These mechanisms also explained the bi-stable deflected and flip-flopped flows with randomly changes from one side to the other as observed by [4], [8], and [9]. Further observation by [3] for two side-by-side cylinders ($T^* = 1.5$) at $x^* = 10$ showed that a row of weak vortices and another peculiar flow pattern were apparent. Such a peculiar pattern was diminished after $x^* = 20$, suggesting that the vortex regeneration or evolution was probably completed [3]. The two-cylinder case for $T^* = 1.7$ may bear a resemblance to that for $T^* = 1.5$ as they are in the same regime of the intermediate cylinder spacing ($T^* = 1.2$-2.0).

Whereas the vorticity contours for $T^* = 1.7$ have a relatively more organized vortex pattern at $\alpha = 0°$, they become scattered with the increase ofα. The maximum contour values of $\widetilde{\omega}_z^*$ are 0.14, 0.08, 0.08 and 0.06 at α = 0°, 15°, 30° and 45°, respectively, representing adecreasing trend as α is increased, especially when $\alpha = 45°$. The non-organized vortex patterns of $\widetilde{\omega}_z^*$ may suggest that the vortex in the wake region of $x^* = 10$ is still not stable. This supports the flow visualization results by [6] behind two side-by-side cylinders for $T^* = 1.5$, who showed that the vortex regeneration or evolution was complete yet at $x^* = 10$. There is also another speculation that the vortices in the narrow wake coalesce with those in the wide wake [3]. In comparison of the $\widetilde{\omega}_x^*$, $\widetilde{\omega}_y^*$ and $\widetilde{\omega}_z^*$ contours, it is obvious that the magnitudes of all coherent vorticity components at each yaw angle are comparable (ranging from 0.06 to 0.12), indicating a more three-dimensional characteristic of the flow. This result is consistent with that shown in Fig.2. With increasing α, the maximum contour values of $\widetilde{\omega}_y^*$ and $\widetilde{\omega}_z^*$ tend to be comparable, especially when α = 30° and 45°. This is consistent with the results shown in Figs. 4 (b), (d) that with the increase of α to 45°, the energy spectra of the transverse and spanwise velocity components are almost comparable. This confirms that the transverse and spanwise vorticities are likely to have similar magnitudes and strength when α is increased to large yaw angles. When $\alpha = 45°$, the maximum contour values of $\widetilde{\omega}_x^*$, $\widetilde{\omega}_y^*$ and $\widetilde{\omega}_z^*$ are comparable (≈ 0.06). This shows that at large yaw angle, the vortices behave strongly three-dimensional, as the strengths of vortices for all components are close to each other. This result should also be related to the large values of $\overline{W}$ for $T^* = 1.7$. Whereasthe maximum contour values of $\widetilde{\omega}_z^*$ decay by 50% when α is increased from 0° to 45°, the change of $\widetilde{\omega}_x^*$ with α for $T^* = 1.7$ is not as apparent as the former. This result indicates a strong interaction between the wake structures when $T^* = 1.7$. It is also evident that vortex contours at $\alpha = 45°$ have a phase variation of about $\phi = 0.5\pi$ compared with those at $\alpha < 40°$. The maximum contour values of $\widetilde{\omega}_x^*$, $\widetilde{\omega}_y^*$ and $\widetilde{\omega}_z^*$ at different yaw angles for $T^* = 1.7$ are also summarized in Table I.

IV. Conclusions

Experiments on wake characteristics of two cylinders in side-by-side arrangement with centre-to-centre spacing ratios of $T^* = 3.0$ and 1.7 at yaw angles $\alpha = 0°$, 15°, 30° and 45° have been conducted. It has been found that the characteristics of the turbulent wakes depend both on the cylinder spacing ratio and the yaw angle.

For $T^* = 3.0$, there exist two vortex streets and the cylinders behave as independent and isolated ones.Asingle peak is observed in the energy spectra, which corresponds to the Strouhal number St_N. For $\alpha < 40°$, the Strouhal number St_N, normalised by the velocity component normal to the cylinders, does not depend on α, indicating that the independence principle is applicable to the wake. The velocity profiles suggest that both vortex streets are similar to the single vortex street at$T^* = \infty$.The lateral distance between the vortices for $T^* = 3.0$ is about $3d$. The phase-averaged vorticity contours are comparable with those for $T^* = \infty$ when the whole set of the contours were shifted downward by about $y^* = 1.5$. This result confirms that the wake of two side-by-side cylinders for large cylinder spacing i.e. $T^* = 3.0$ behaves as an independent and isolated cylinder. The maximum coherent streamwise vorticity contours $\widetilde{\omega}_x^*$ is only about 10% of that of the coherent spanwise vorticity contours $\widetilde{\omega}_z^*$. With the increase ofα, $\widetilde{\omega}_x^*$ increases whereas $\widetilde{\omega}_z^*$ decreases, especially when $\alpha = 30°$. At $\alpha = 45°$, $\widetilde{\omega}_x^*$ is about 67% of $\widetilde{\omega}_z^*$. This result indicates the existence of the secondary axial vortices or the occurrence of the vortex dislocation with an enhanced three-dimensionality at larger

α.On the other hand, the maximum magnitude of $\widetilde{\omega}_y^*$ is independent of α.

For $T^* = 1.7$, only a single peak is detected onϕ_v. This is because at $x^* = 10$, the vortex structure regeneration or evolution may not be completed yet, whereas those in the narrow wake are probably diminished before this downstream location. The independence principle (IP) is also applicable to the wake when $\alpha < 40°$. The spanwise vorticity contours have an organized pattern at $\alpha = 0°$ whereas becoming scattered and smaller with the increase of yaw angle. With increasing α, there is a decreasing trend in the maximum vorticity contours. The less organized $\widetilde{\omega}_z^*$ contours for $T^* = 1.7$ compared with those for $T^* = \infty$ and 3.0 indicate that the vortex motion in the wake is still not stable, suggesting that the vortex evolution or regeneration process may not be completed yet. At $\alpha = 45°$, the vortices show apparent three-dimensionality as the maximum contours of the three vorticity components are very comparable. Furthermore, the vorticity contours at $\alpha = 45°$ have phase variation of about 0.2π compared with that at smaller yaw angles. The maximum coherent vorticity contours of $\widetilde{\omega}_x^*$ and $\widetilde{\omega}_z^*$ for $T^* = 1.7$ are about 30% and 7% of those for $T^* = 3.0$. This result suggests that the coherent vorticity components for $T^* = 1.7$ are much weaker than those of both $T^* = 3.0$ and the single cylinder wake.

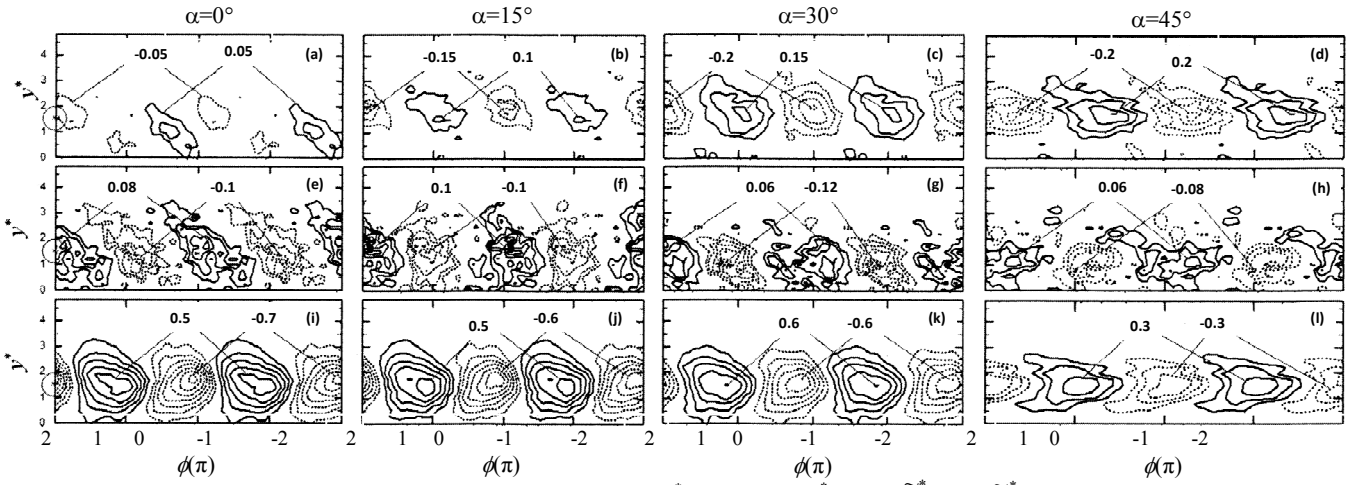

Fig. 7 Phase-averaged vorticity components at different yaw angles for $T^* = 3.0$. (a-d) $\widetilde{\omega}_x^*$; (e-h) $\widetilde{\omega}_y^*$; (i-*l*) $\widetilde{\omega}_z^*$. (a-d) Contour interval = 0.05; (e-h) 0.02; (i-l) 0.10. $\phi = 2\pi$ corresponds to the λ ($\equiv U_c/f_0$). The open circles with a cross at the centre represent the locations of the cylinders.

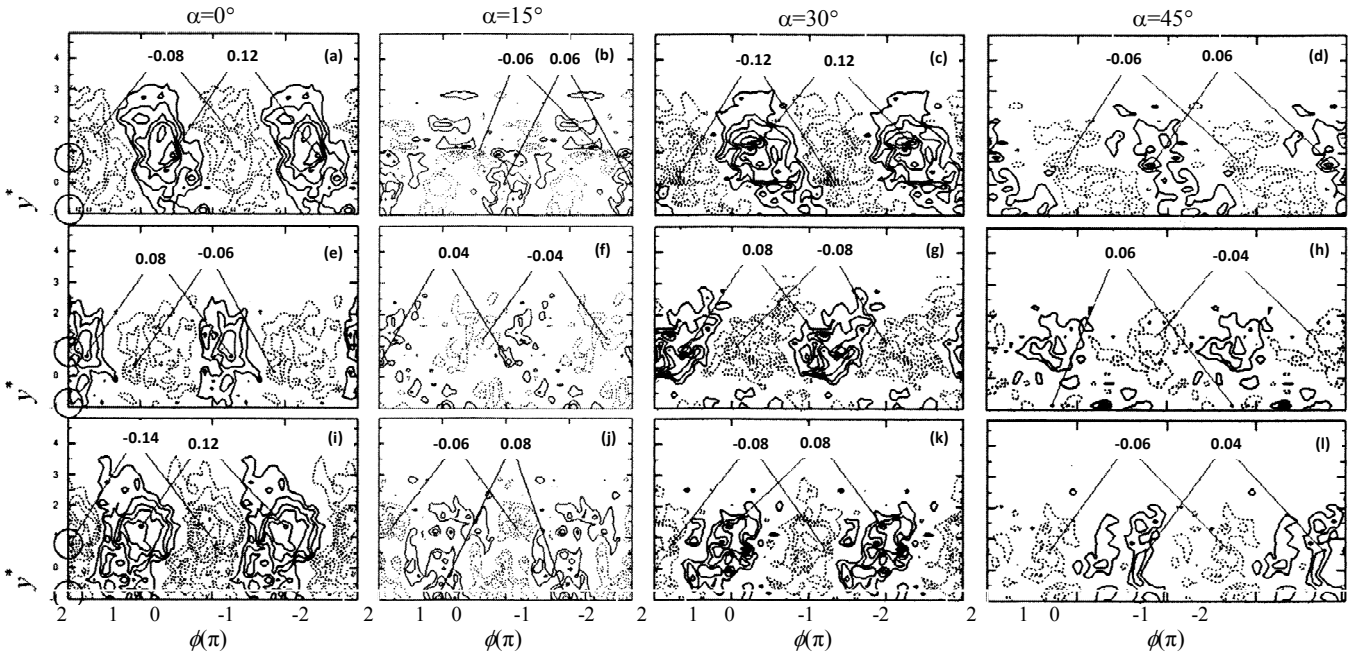

Fig. 8 Phase-averaged vorticity components at different yaw angles for $T^* = 1.7$. (a-d) $\widetilde{\omega}_x^*$; (e-h) $\widetilde{\omega}_y^*$; (i-*l*) $\widetilde{\omega}_z^*$. (a-*l*) Contour interval = 0.02. $\phi = 2\pi$ corresponds to the $\lambda/2$ ($\equiv U_c/2f_0$). The open circles with a cross at the centre represent the locations of the cylinders

REFERENCES

[1] Mahir, N. and D. Rockwell, Vortex formation from a forced system of two cylinders. Part II: Side-by-side arrangement, Journal of Fluids and Structures, vol. 10, 1996,pp. 491-500.
[2] Zdravkovich, M.M., Review of flow interference between two circular cylinders in various arrangements, Journal of Fluids Engineering, vol. 99, 1977,pp. 618-633.
[3] Zhou, Y., H.J. Zhang, and M.W. Yiu, The turbulent wake of two side-by-side circular cylinders, Journal of Fluid Mechanics, vol. 458, 2002,pp. 303-332.
[4] Bearman, P.W. and A.J. Wadcock, The interaction between a pair of circular cylinders normal to a stream, Journal of Fluid Mechanics, vol. 61, 1973,pp. 499-511.
[5] Zhou, Y., Wang, Z.J., So, R.M.C., Xu, S.J. and Jin, W. Free vibrations of two side-by-side cylinders in a cross-flow, Journal of Fluid Mechanics, vol. 443, 2001,pp. 197-229.
[6] Williamson, C.H.K., Evolution of a single wake behind a pair of bluff bodies, Journal of Fluid Mechanics, vol. 159, pp. 1985, 1-18.
[7] Chen, L., J.Y. Tu, and G.H. Yeoh, Numerical simulation of turbulent wake flows behind two side-by-side cylinders, Journal of Fluids and Structures, vol. 18, 2003,pp. 387-403.
[8] Ishigai, S., Nishikawa, E., Nishmura, K., Cho, K, Experimental study on structure of gas flow on tube banks with tube axes normal to flow, Part 1, Karman vortex flow from two tubes at various spacing ratios, Bulletin of Japan Society of Mechanical Engineers, vol. 15, 1972,pp. 945-956.
[9] Kim, H.J. and P.A. Durbin, Investigation of the flow between a pair of circular cylinders in the flopping regime, Journal of Fluid Mechanics, vol. 196, 1988,pp. 431-448.
[10] Sumner, D., Wong, S.S.T, Price, S.J. and Païdoussis, M.P., Fluid behaviour of side-by-side circular cylinders in steady cross-flow, Journal of Fluids and Structures, vol. 13, 1999,pp. 309-338.
[11] Alam, M.M. and Y. Zhou, Turbulent wake of an inclined cylinder with water running, Journal of Fluid Mechanics, vol. 589, 2007,pp. 261-303.
[12] Surry, D. and J. Surry, The effect of inclination on the Strouhal number and other wake properties of circular cylinders at subcritical Reynolds numbers, in Technical Report. 1967, UTIAS TechnicaI Institute for Aerospace Studies, University of Toronto.
[13] Zhou, T., Razali, S.F.Mohd, Zhou, Y., Chua, L.P. and Cheng, L., Dependence of the wake on inclination of a stationary cylinder, Experiments in Fluids, vol. 46, 2009,pp. 1125-1138.
[14] Marshall, J.S., Wake dynamic of a yawed cylinder, Journal of Fluids Engineering, vol. 125, 2003,pp. 97-103.
[15] Hoerner, S.F., Fluid-dynamic drag: Practical information on aerodynamic drag and hydrodynamic resistance. 1965: Hoerner Fluid Dynamics. pp. 3-11.
[16] Schlichting, H., Boundary-layer theory. 7th ed. ed. 1979, New York: McGraw-Hill.
[17] Hanson, A.R., Vortex shedding from yawed cylinders, AIAA Journal 4, 1966,pp. 738-740.
[18] Van Atta, C.W., Experiments on vortex shedding from yawed circular cylinders, AIAA Journal, vol. 6, no. 5, 1968,pp. 931-933.
[19] King, R., A review of vortex shedding research and its application, Ocean Eng, vol. 4, 1977,pp. 141-171.
[20] Ramberg, S.E., The effect of yaw and finite length upon the vortex wakes of stationary and vibrating circular cylinders, Journal of Fluid Mechanics, vol. 128, 1983,pp. 81-107.
[21] Kozakiewicz, A., J. Fredsøe, and B.M. Sumer. Forces on pipelines in oblique attack: steady current and waves. In Proceedings of the fifth international offshore and polar engineering conference. 1995. The Hague, The Netherlands: The International Society of Offshore and Polar Engineers.
[22] Lucor, D. and G.E. Karniadakis, Effects of oblique inflow in vortex-induced vibrations, Flow, Turbulence and Combustion, vol. 71, 2003,pp. 375-389.
[23] Thakur, A., X. Liu, and J.S. Marshall, Wake flow of single and multiple yawed cylinders, Journal of Fluids Engineering, vol. 126, 2004, pp. 861-870.
[24] Smith, A.R., W.T. Moon, and T.W. Kao, Experiments on flow about a yawed circular cylinder, Journal Basic Engineering, vol. 94, 1972, pp. 771-777.
[25] Kiya, M. and M. Matsumura, Turbulence structure in intermediate wake of a circular cylinder, Bulletin of Japan Society of Mechanical Engineers, vol. 28, 245, 1985,pp. 2617-2624.
[26] Zhou, T., Wang, H., Razali, S.F. Mohd., Zhou, Y. and Cheng, L.Three-dimensional vorticity measurements in the wake of a yawed circular cylinder, Physics of Fluids, vol. 22, 2010, 015108.
[27] Matsumoto, M., N. Shiraishi, and H. Shirato, Rain-wind induced vibration of cables of cable-stayed bridges, Journal of Wind Engineering and Industrial Aerodynamics, vol. 43, 1992,pp. 2011-2022.
[28] Hammache, M. and M. Gharib, An experimental study of the parallel and oblique vortex shedding from circular cylinders, Journal of Fluid Mechanics, vol. 232, 1991,pp. 567-590.
[29] Mansy, H., P.-M. Yang, and D.R. Williams, Quantitative measurements of three-dimensional structures in the wake of a circular cylinder, Journal of Fluid Mechanics, vol. 270, 1994, pp. 277-296.
[30] Zhang, H.J. and Y. Zhou, Effect of unequal cylinder spacing on vortex streets behind three side-by-side cylinders, Physics of Fluids,vol. 13 no. 12, 2001,pp. 3675-3686.